Estuarine, Coastal and Shelf Science 261 (2021) 107556

Contents lists available at ScienceDirect

Estuarine, Coastal and Shelf Science

journal homepage: www.elsevier.com/locate/ecss

The effects of plant structure and flow properties on the physical response of coastal dune plants to wind and wave run-up

Rachel A. Innocenti [a,b,*], Rusty A. Feagin [a,c], Bianca R. Charbonneau [d,e], Jens Figlus [f], Pedro Lomonaco [g], Meagan Wengrove [h], Jack Puleo [i], Thomas P. Huff [a], Yashar Rafati [i], Tian-Jian Hsu [i], Maria V. Moragues [j], Benjamin Tsai [i], Thomas Boutton [a], Maria Pontiki [i], Jeremy Smith [i,k]

[a] Department of Ecology and Conservation Biology, Texas A&M University, College Station, TX, 77843, USA
[b] Environmental Laboratory, U.S. Army Engineer Research and Development Center, Vicksburg, MS, 39180-6199, USA
[c] Department of Ocean Engineering, Texas A&M University, College Station, TX, 77843, USA
[d] Department of Biology, University of Pennsylvania, Philadelphia, PA, 19104, USA
[e] US Department of Defense Army Engineer Research and Development Center, Oak Ridge Institute of Science and Education, Oak Ridge, TN, 37830, USA
[f] Department of Ocean Engineering, Texas A&M University, Galveston, TX, 77553, USA
[g] O.H. Hinsdale Wave Research Laboratory, Oregon State University, Corvallis, OR, 97331, USA
[h] Department of Civil and Construction Engineering, Oregon State University, Corvallis, OR, 97331, USA
[i] Department of Civil and Environmental Engineering, University of Delaware, Newark, DE, 19716, USA
[j] Andalusian Institute for Earth System Research, University of Granada, Avda. del Mediterráneo, s/n, 18006, Granada, Spain
[k] Department of Civil & Environmental Engineering, Stanford University, Stanford, CA, 94305, USA

ARTICLE INFO

Keywords:
Abiotic forces
Ammophila arenaria
Ammophila breviligulata
Bioprotection
Cakile maritima
Flume
Panicum amarum
Storm
Wind tunnel
Drag coefficient
Coastal dunes

ABSTRACT

Vegetation is an important feature of coastal dunes and is often managed to stabilize restored dunes and provide coastal protection. Despite a high investment in planting and management efforts, little is known about how vegetation is affected by wind and wave run-up. The objectives of this study were to 1) investigate the lift forces and drag moments experienced by coastal dune vegetation from wind and wave run-up and 2) relate them to flow properties and plant morphology. *Panicum amarum*, *Ammophila breviligulata*, *A. arenaria* and *Cakile maritima* were subjected to laboratory wind and wave run-up conditions. Measurements were taken of fluid velocity, run-up depth, Reynolds number, and plant biophysical properties. The plant lift and drag responses were recorded with the use of a novel sensor designed to address the complexities induced by the flexibility and morphology of real vegetation under varying conditions. Regression analysis was used to describe the relationships between plant response and plant structure and flow properties. Experiments showed that wind induced a constant lift force and drag moment on plants over time, whereas run-up induced plant response was time-dependent. Plant height ($R^2 = 0.64$, $p < 0.001$) and number of leaves ($R^2 = 0.67$, $p = 0.30$) were the most important predictors of drag moment from wind and run-up experiments, respectively. Plant drag coefficients from wind (5.0×10^{-4} to 3.6×10^{-2}) and run-up (2.7×10^{-3} to 1.7) were negatively correlated with flow turbulence, indicating that coastal dune plants likely have biophysical adaptations to the induced forces, such as a propensity for streamlining. In particular, our data suggests that tall and thin dune grasses are best adapted and used on the dune crest and fronts to mitigate wind energy, while low shrubby plants are best used on the backbeach or dune toe to reduce run-up energy. Our study provides valuable information on the ability of dune vegetation to interrupt flow, such that modelers and managers can better understand how to best protect coastlines.

1. Introduction

Nature-based solutions have become popular for protecting coastal infrastructure from wind and waves (French, 2001; Temmerman et al., 2013; Charbonneau, 2015; Elko et al., 2016, Odériz et al., 2020). For some applications, these solutions can even provide successful

* Corresponding author. Coastal Ecology and Management Laboratory, Dept. Ecology and Conservation Biology, Texas A&M University, 77843, USA.
E-mail address: r.innocenti@outlook.com (R.A. Innocenti).

https://doi.org/10.1016/j.ecss.2021.107556
Received 12 November 2020; Received in revised form 7 July 2021; Accepted 13 August 2021
Available online 20 August 2021

alternatives to hard, engineered structures (Harman et al., 2015; Williams and Gutierrez, 2009). Coastal dunes in particular can protect coastal communities during high tides and storm events (Feagin et al., 2015; Sigren et al., 2018), while also providing other valuable ecosystem services (Barbier et al., 2011; Everard et al., 2010; Koch et al., 2009).

Dunes constructed as nature-based coastal defenses are vegetated to reduce dune erosion. The aboveground and belowground structures of vegetation may alter erosion through biological and physical processes. Biologically, plants directly and indirectly improve soil stability through the addition of exudates and dead organic matter (Feagin et al., 2009; Naveed et al., 2018). Physically, vegetation interacts with erosive wind and water forces by inducing drag on flow fields, thereby reducing the energy available to mobilize sediments (Hesp, 2013; Fang et al., 2018). The amount of drag a plant contributes to wind or water flow is affected by the plant structure (Albayrak et al., 2012; Lei and Nepf, 2019; Luhar and Nepf, 2016; Vogel, 1984), and can be described by the drag coefficient (Tanaka et al., 2011; Tsakiri et al., 2016; Jeon et al., 2018; Zhang et al., 2017), which encapsulates all of the complex dependencies of plant shape, inclination, and flow conditions on drag. This parameter can also be helpful to understanding plant response to flow, since it includes the effects of form drag, and can indicate flow induced plant reconfiguration, such as streamlining (Vogel, 1984). While drag coefficients have been estimated for coastal wetland vegetation (Hijuelos et al., 2019, Gijón Mancheño et al., 2021; Zhang et al., 2020, Baron--Hyppolite et al., 2019), coastal dune vegetation has been largely ignored, despite its importance to the services and resiliency of protective coastal dunes.

Wind and run-up conditions experienced by coastal dune plants differ greatly in terms of fluid density, flow structure, boundary layer interactions, and inertial versus drag effects. Previous studies on vegetation in relation to wind and water conditions mostly fall into two categories: those that consider the effects of the physical forces on plants, and those that study the effect of the plants on the forces. Studies which fall into the first group, primarily focus on unilateral flow fields (Cao et al., 2012; Borisevich and Vikhrenko, 2018; Kothyari et al., 2009; Hui et al., 2010). However, the water energy intercepted by dune plants is most often from run-up bores, in which the water velocity at a single point is constantly changing. As a result, these studies are difficult to apply to dune vegetation. Other research considers oscillatory wave energy, and falls into the second category, focusing on the effect of submerged (Kobayashi et al., 1993; Myrhaug, 2019; Lou et al., 2018; Zhu et al., 2020; Chen and Zou, 2019) and emergent (Huang et al., 2011; Yin et al., 2019; Jacobsen et al., 2019) vegetation on wave energy. This disjunction leaves researchers to make assumptions about the energy experienced by the plants. Moreover, most studies from both categories use wooden or plastic dowels as representatives of plants, avoiding the complexity of real vegetative structures, and causing further problems as drag characteristics are strongly influenced by the shape of the idealized vegetation (Thompson et al., 2003).

The overall objective of this study was twofold: to investigate the physical effects of wind and run-up forces on dune plants, and to relate exerted force to flow properties and plant traits. Specific objectives were to (1) assess the spatial, temporal, and magnitude differences between wind and run-up induced forces and moments on dune plants, (2) determine the relationship between flow properties and plant biophysical traits on exerted force, and (3) describe the drag effects by calculating plant drag coefficients across varying flow turbulences, for different plant types. Physical disturbance from wind and run-up is characteristic of dune ecosystems. We offer that by considering the physical conditions to which dune plants are exposed alongside dune plant biophysical traits, we can better understand potential plant strategies to dealing with physical disturbances and improve the effectiveness and resiliency of ecosystem-based features for coastal protection.

This study also took a unique experimental approach and focused primarily on comparing drag moments as opposed to drag forces (Butler et al., 2012; Loboda et al., 2018; Wilson et al., 2008). This is a novel approach, which allowed us to consider the more common phenomena endured by plants: rotation about their stem axis where the stem meets the ground. This approach also had the benefit of integrating complex motion and flow reconfiguration of real plants into moment measurements.

2. Methods

A sensor capable of detecting drag moment and lift force experienced by an individual plant was constructed, and plants from several dune species were tested in the laboratory with a series of wind and run-up conditions. Correlations between force, moment, and flow turbulence and plant biophysical traits were identified, and plant drag coefficients were calculated. These data were synthesized to describe how dune plants differentially respond to wind versus wave run-up phenomena.

2.1. Force sensor design and calibration

A sensor capable of detecting drag and lift forces experienced by an individual plant was created using a series of strain gauges (Supplemental Figure Ia). The sensor was constructed from a square steel base frame, with two 2 mm thick stainless-steel bars spanning the frame (these bars were relatively thin and thus sensitive). Plants were glued using epoxy into a steel sleeve (diameter, 12.7 mm; height, 38.1 mm), and this sleeve was then mounted with screws into a mounting cup that was welded to an adjoining plate. The plate was then attached to the 2 mm stainless-steel bars using bolts at a consistent torque. The arrangement allowed no movement between the component parts, and the central part can be assumed as a rigid body, such that all force on the plant produced deflection in the bars (Supplemental Figure Ib). Steel was used due to its physical properties (Modulus of Elasticity, 193 GPa; Ultimate Tensile Strength, 505 MPa; Brinell Hardness, 123), consistency of deflection, and compatibility with the strain gauges. A total of four Kyowa waterproof strain gauges (Type: KFWS-2N-120-C1-11L3M2R) were arranged on the bars to detect their bending when force was applied to the mounted plant specimen. One strain gauge was placed on the top and bottom of each bar (total of four strain gauges) to constitute two, half-bridge Wheatstone bridges in the 2-active-gauge method. This configuration allowed for temperature compensation and to cancel the detection of compressive/tensile strain. Finally, two Bridge Completion Modules (BCM-1, Omega Engineering, Inc.) were added to complete the half-bridges and eliminate the need for a potentiometer.

Calibration equations were derived for the strain gauge array on each bar to convert voltage outputs to force. To calibrate, various weights were placed atop the sensor's sleeve five separate times, and the average voltage measurement for each weight was normalized to the average baseline output (taken without a loading). The normalized voltages were regressed against the force of gravity on the weights (calculated from Newton's second law: $F_g = m*g$), and the equation from the regression was used to calculate force for a given voltage output. In this manner, a quantitative relationship was established between lift force and the voltage response for each bridge, and consequently, each bar.

The calibration equations were derived for each bar separately. Due to the method of calibration, positive and negative voltages indicated a force applied in an upward or downward direction, respectively. This characteristic of our sensor allowed us to identify lift force that is exerted upward and downward (both bars measuring force in the same direction), and drag moment leveraged in the clockwise and counterclockwise direction relative to the horizontal plane (front bar measuring positive force and back bar measuring negative force, or vice versa). Drag moment was calculated using the following equation:

$$M = (F_1 - F_2)*(d/2) \quad (1)$$

where F_1 is the force measured by the front beam, F_2 is the force

measured by the back beam, and (*d/2*) is half the distance between the two point forces (Supplemental Figure Ib). The sensor did not record data in the alongshore direction (laterally side to side), perpendicular to the exerted wind or wave-run up.

The distance between the two point forces was the length of the plate connecting the 2 bars of the force sensor, since it was at these points the applied force was transferred from the plant to deflect the bars and produce a voltage change. This design element of our sensor prevented us from having to calculate the lever length as a function of the plant. The identification of a plant-based length would be difficult in the context of a flexible plant with a potentially complex shape, and would be further complicated by correlations between these quantities and the changing velocities of wind. Tanaka et al. (2011) suggested a simplifying assumption to identify *d* for a tree, using the summation of the height of the lowest branch and one-third of the crown height. Our sensor avoided making these assumptions, because the lever was the plate, it had a known and fixed length, and its rotation was driven by forces applied to the plant. Essentially, a moment exerted on the plant (complicated by the changing and correlated factors listed above) was orthogonal yet equivalent to a moment exerted on the plate (which had a known and unchanging length, was inflexible, and thus allowed a consistent determination of the moment with measurement of the forces).

2.2. Wind tunnel set-up

To measure lift forces and drag moment on dune plants at various wind conditions, we used the Ocean County Vocational Technical School moveable bed, unilateral flow wind tunnel (Fig. 1a). Details on the wind tunnel specifications can be found at thewindtunnel.weebly.com. A WindMaster 3D sonic anemometer (Gill Instruments, Inc.; Range: 0 m/s - 50 m/s; Accuracy: <1.5% RMS at 12 m/s) was placed 30 cm away from the nearest chamber wall and 20 cm to the side of the plant and force sensor to monitor wind velocity at the location of the plant (Supplemental Figure IIa). The height of the anemometer was 38.5 cm for *P. amarum* and *A. breviligulata* experiments and 20 cm for *C. maritima* experiments due to differences in plant heights and to keep the anemometer at a relevant location for all plants. The anemometer and force sensor were connected to a data logger (DI-718B, Dataq Instruments, Inc.) set at a sampling rate of 100 Hz to synchronize data collection. To reduce the interference of the wind flow, the base of the force sensor was recessed beneath the chamber floor and the specimen extended up into the chamber through a hole in the floor (Supplemental Figure IIb). The mounting portions of the 3D anemometer were also placed beneath the chamber floor and extended up through another hole and sealed. The 3D anemometer was located outside of the boundary layer of the force sensor and plants to avoid flow disruption (Supplemental Figures III and IV). Similarly, both the sensor and plant were well outside the ceiling and side wall boundaries of the wind tunnel chamber. We determined the bed-level boundary layer to begin at ~20 cm due to a substantial drop in wind speed at this height observed in the vertical velocity profile. The boundary layer height is relevant because within this layer the affective wind speed the plants experience is reduced, as we address in the *Discussion* section below.

2.3. Wave flume set-up

To simulate run-up forces exerted on dune vegetation, we tested plants in the force sensor as part of a larger project on dune erosion at the Large Wave Flume (LWF) at Oregon State University (Fig. 1b). A prototype beach and dune profile were constructed in the flume (beach-dune profile dimensions: 4.5 m tall, 70 m long, 3.7 m wide), and the dune was vegetated with *P. amarum* as part of the experiment. The plant -force sensor unit was placed between the crest of the berm and the front edge of the vegetation at different times during the context of the project. As the beach-dune profile changed, the exact location of the force sensor was also changed to capture plant interaction with run-up, formed after the waves had broken, turned into bores, and rushed up the slope of the beach/dune. The force sensor was attached to a steel plate which was suspended from an arm extending from the flume wall (Supplemental Figure Va). Mounted 60 cm and 15 cm alongside the force sensor were an Ultrasonic sensor (Banner Engineering, Inc. Range: 300 mm- 3 m; Response time: 135 ms) and an Acoustic Doppler Velocimeter (ADV, Vectrino, Nortek, Inc.; Range: ± 2.5 m/s; Accuracy: ±0.5% of measured value ± 1 mm/s) to measure run-up water level and water velocity at the location of the test plant, respectively. The Ultrasonic wave gauge, ADV, and force sensor were connected to a data logger (DI-718B, Dataq Instruments, Inc.) set at a sampling rate of 100 Hz to synchronize data collection, as in the wind tunnel experiments. A

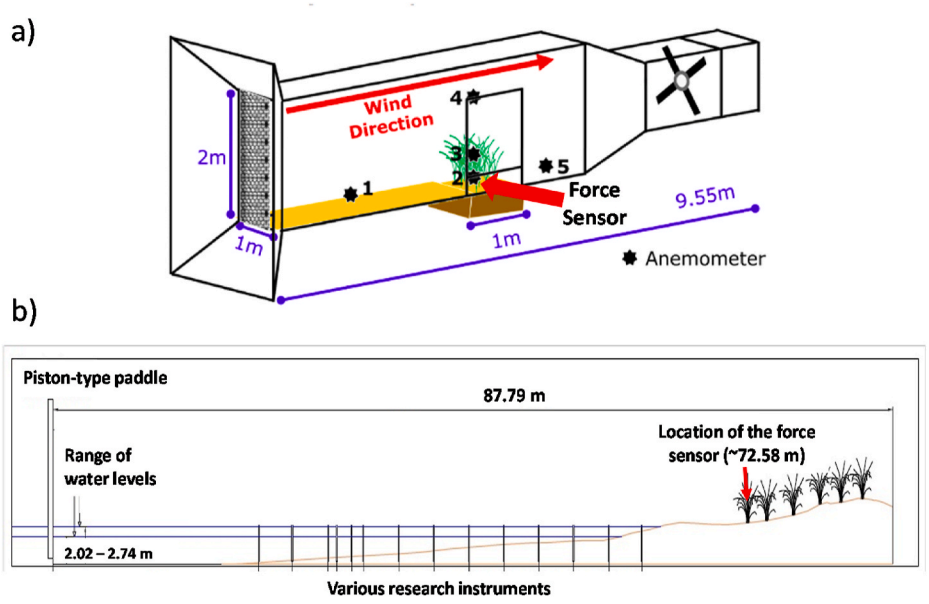

Fig. 1. Diagram of the (a) wind tunnel and (b) the Large Wave Flume set-up in the Hinsdale Wave Lab at Oregon State University. For the LWF diagram, distances in the x-direction are measured from the piston-type wave paddle (x = 0 m). For the run-up experiments, the force sensor-plant unit was placed at the front edge of vegetation (~72.58 m) and was moved in congruence with changes to experimental water level in order to capture plant interaction with run-up.

protective box encapsulated the force sensor to prevent run-up from directly applying force to the sensor and to ensure only forces applied to the mounted plant were measured (Supplemental Figure Vb). The force sensor and the steel plate were buried to prevent flow interference, similar to the wind tunnel experiments. No sediment touched the base of the plant to allow it to move freely as it was intercepted by run-up.

2.4. Wind and run-up test conditions

For wind experiments, we tested each plant with five wind conditions: (1) 2.2 m/s, (2) 4.5 m/s, (3) 6.7 m/s, (4) 8.9 m/s and (5) 11.2 m/s. We chose these wind speeds to simulate a beach environment and to capture changes in applied force from subtle changes in wind speed. The observed wind velocities were: (1) 2.23 ± 0.07 m/s; (2) 4.39 m/s ± 0.10; (3) 6.54 m/s ± 0.18; (4) 8.84 m/s ± 0.19; (5) 11.03 m/s ± 0.29 m/s. For each trial of each plant, velocity, forces, and moments were averaged over a duration of 30 s and used for subsequent statistical analysis.

For run-up experiments, we tested several conditions representative of those occurring during a storm-event, by creating irregular waves based on a TMA shallow water spectrum (Bouws et al., 1985). Our sampling occurred specifically across these conditions: significant wave heights (Hs) 0.73 m–0.89 m, peak wave period (Tp) 5.05 s–6.07 s, and water level (h) 2.15 m–2.31 m. Data from the experiments was a time series of water level, velocity, and force. Data points were selected based on the signal to noise ratio (SNR) calculated from the ADV data, such that if the SNR of velocity in the u direction was less than 10, all data points were removed for that time period. Since the duration of each trial was greater than 30 min, this helped us isolate run-up events within each time series. For analysis, we isolated ten run-up events for each plant where the run-up intercepted the plant. We selected run-up events that occurred early in each trial to avoid effects from declined structural integrity of the plants due to the duration of each trial and constant interception from run-up. Additionally, the sequence of uprush and backwash caused plants to experience a sequence of negative and positive forces and moments as a wave surged landward and then receded seaward. As a result, we chose to focus on the initial arrival of run-up, and thus our force and hydrodynamic measurements were limited to, and then averaged over, the first second of interception. Bubbles present in the front of the swash bores were removed with the filtering described above, and so did not affect this first second average. The observed average water velocity in the landward-direction within the run-up bores was 0.64 m/s ± 0.28 m/s and ranged from <0.1 m/s- 1.21 m/s. The observed average run-up water depth was 4.63 cm ± 3.54 cm and ranged from 0.31 cm to 20.46 cm.

For both wind and run-up cases, we calculated Reynold's number, Re, as an indicator of flow turbulence. The following equation was used:

$$Re = \frac{UL}{v} \tag{2}$$

where U is the average velocity of the fluid, L is a length scale, and v is the kinematic viscosity of the fluid. We calculated Re for each experimental trial. For wind experiments, v for air was 1.48×10^{-5} m^2/s and for water experiments, v was 1.05×10^{-6} m^2/s. The length scale was taken as the average stem diameter of all plants used in the study to allow flow turbulence comparisons between wind and run-up trials.

2.5. Plant biophysical traits

We conducted wind and run-up experiments on the following species: American beachgrass (*Ammophila breviligulata*), European beachgrass (*A. arenaria*), Bitter panicgrass (*Panicum amarum*), and Sea Rocket (*Cakile maritima*; Fig. 2). The plants used for run-up experiments were collected from naturally established vegetation stands in the backshore and dunes of Newport, Oregon (44.6368° N, 124.0535° W), and those collected for the wind experiments were collected from Delaware State Seashore, Delaware (38.7209° N, 75.0760° W). All plants were collected between May and October when the plants were fully grown. *A. arenaria* was from Oregon for run-up experiments, and *A. breviligulata* was from Delaware for wind experiments; the two species were relatively similar in height and other morphological characteristics (Fig. 2). The *P. amarum* plants used for run-up experiments were collected from the dune constructed for the larger LWF experiment. These plants were grown for three months within a greenhouse atop the dune maintained at 80 °F. For our study, ten plants of each species were used for wind experiments, and a separate four plants of each species were used for run-up experiments. For run-up experiments, the duration of the trials (30 min) caused many of the plant stems to eventually fail from constant run-up interception. As a result, from the run-up experiments, only two plants from each species had sufficient data to be analyzed (Table 1).

We measured the following biophysical traits for each individual plant: plant height, stem diameter, volume, number of leaves, stem modulus of elasticity (E), wet biomass, and frontal area (Table 2). Plant height was recorded with the plant lying flat, starting at the point on the tiller above which no more roots were present. Volume was measured after the plant underwent experimental conditions by submerging the entire plant in water and recording the volume of water displaced by the plant. The Young's modulus of elasticity of each plant stem was calculated by conducting simple beam loading experiments, following Feagin et al. (2011). Simple beam theory states that Young's modulus, E, is proportional to the slope of applied load (F) versus deflection (y), such

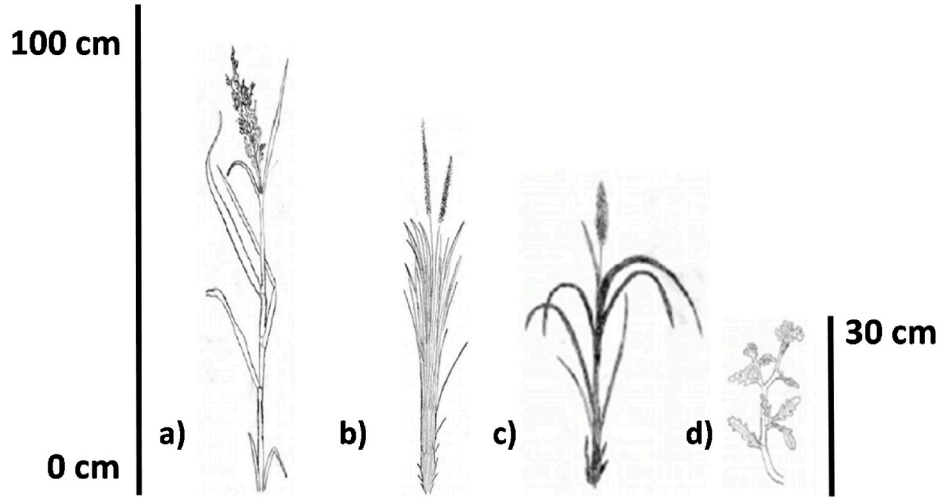

Fig. 2. Representative individuals of (a) *P. amarum*, (b) *A. breviligulata*, (c) *A. arenaria*, and (d) *C. maritima* used for wind and run-up experiments.

Table 1
The number of plants, experimental conditions, and the resulting replicates considered for data analysis.

Experiment	Number of individuals per species	Number of experiments per individual	Number of experiments per species	Number of replicate experiments per individual	Number of replicate experiments per species
Wind	10	5	50	0	10
Run-up	2	10	20	0	2

Table 2
Average measured biophysical traits for each species. 'Wet AG biomass' represents wet above ground biomass. Volume was not measured for plants from run-up experiments.

Wind Experiments							
Species	Height (cm)	Stem Diameter (cm)	Volume (cm^3)	Number of leaves	Stem E (N/cm^2)	Wet AG biomass (g)	Frontal area (cm^2)
Ammophila breviligulata	71.2±	0.75±	7.7±	5.4±	1.9E5±2.0E5	4.4±	25.9±
	5.2	0.2	1.3	1.0		2.4	16.1
Panicum amarum	115.0 ± 10.7	0.48±	20.0±	5.1±	4.5E6±4.2E6	5.7±	114.5±
		0.1	3.5	1.0		2.4	41.8
Cakile maritima	20.0±	0.57±	21.3±	15.8±	1.3E5±8.1E4	13.3±	102.1±
	8.2	0.1	8.8	8.7		4.6	39.6
Run-up Experiments							
Species	Height (cm)	Stem Diameter (cm)	Volume (cm^3)	Number of leaves	Stem E (N/cm^2)	Wet AG biomass (g)	Frontal area (cm^2)
Ammophila arenaria	67.0±	0.55±	-	6.0±	4.7E6±	2.8±	63.4±
	5.7	0.5		4.9	6.5E6	2.1	42.8
Panicum amarum	26.6±	0.55±	-	16.3±	1.1E6±9.8E4	4.5±	113.7±
	4.2	0.07		13.4		2.1	116.5
Cakile maritima	31.8±	0.75±	-	78.3±	9.4E4±	30.0±	141.1±
	4.9	0.07		24.0	2.9E4	8.5	3.8

that:

$$E = \frac{\sigma}{\varepsilon} = \left(\frac{L^3}{48I}\right)\left(\frac{F}{y}\right) \tag{3}$$

where L is beam length, I is moment of inertia, and (F/y) is the slope found by linear regression of measured F and y. Young's modulus indicates flexibility, and a smaller value corresponds with a more flexible material. Finally, frontal area was calculated using ImageJ image processing software, available online by the National Institutes of Health (Rasband and ImageJ, 1997).

2.6. Drag coefficient calculation

We calculated the drag coefficient for each species using the steady flow portion of the Morison equation:

$$C_D = \frac{F_D}{\frac{1}{2}\rho U^2 A} \tag{4}$$

where C_D = drag coefficient, F_D = drag force experienced by the plant, ρ = density of the fluid (air or water), U = mean channel flow velocity, and A = area of the plant projected in the stream-wise direction and affected by the flow (Morison et al., 1950). For unsteady flows the total force also incorporates an inertial term, however this was not included for our study (see *Discussion* section *Fluid flow properties and exerted forces*).

Drag force, F_D, was calculated differently for wind and run-up experiments. For both wind and run-up experiments, we assumed the flow applied a uniformly distributed load to the plant for simplification. Thus, we calculated F_D by dividing the drag moment (measured by the force sensor) by the length of the moment arm divided by two ($d/2$). For wind experiments, $d/2$ was the plant height, as the plant was fully immersed in the wind (see *Wind tunnel set-up*). For run-up experiments, we had to account for the variable depth of run-up bores affecting the amount of plant influenced by the flow. Thus, we calculated F_D by multiplying the drag moment by one half of the water depth, which allowed us to ignore the length of the plant extending above the run-up, unaffected by flow.

Similarly, we calculated the frontal area of the plant affected by the flow, A, differently for wind and run-up experiments. For wind experiments, we used the entire plant frontal area to calculate C_D. For run-up experiments, we calculated A by multiplying the plant frontal area by the ratio of run-up water depth to plant height. This ratio represents the proportion of plant area submerged and affected by run-up, assuming that the plant's total cross-sectional area is evenly distributed down the height of the plant, such as a cylinder. For the *P. amarum* and *A. arenaria* grasses we tested, stem and leaf structure was generally homogenous down the stem axis. For the *C. maritima* individuals we tested, plants were shorter and wider with more heterogeneous structure so that their front was more circular compared to the grass species. However, many of the *C. maritima* plants were short enough that run-up completely submerged the plant, making plant height:run-up depth equal to 1, and the total frontal area was used to calculate C_D. We calculated A separately for every run-up event for each plant. By using the methods described above to calculate F_D and A, we were able to consider only the part of the plant affected by flow and calculate a more accurate estimate for C_D. Finally, ρ was 1.23 kg/m^3 and 997 kg/m^3 for air and water, respectively.

2.7. Data analysis

For both wind and run-up cases, we statistically regressed the measured lift force and drag moment against the wind velocity, water velocity, and water depth for each species. We also regressed measured force and moment against *Re* for each species. The goodness-of-fit was determined using R^2, and its significance, using p values.

To assess the relationship between wind and run-up drag moment and lift forces and plant biophysical traits, we performed univariate regression using R Studio (R Core Team, 2019; R version 3.5.3). For these regressions, we only used the moment and force measurements from the trials of the strongest conditions. Since the strongest conditions experienced by each species varied for wind and run-up experiments, we binned wind velocity between 10.8 m/s - 11.2 m/s and run-up water level between 3 cm and 5 cm of depth (water velocities 0.87 m/s −1.16 m/s) and used the corresponding force data for regression. Regression was performed using the data for each species individually for the wind experiments; however, there were too few plant replicates to consider

each species separately for the run-up experiments (Table 1). As a result, for run-up experiments, we performed simple linear regression on plant response and plant trait data from all species combined. Finally, stepwise multiple regression was performed with the combined data from all the species for wind and run-up conditions, separately. By combining the data, we were able to generalize our analysis and determine plant traits most correlated with affects from wind and run-up.

For the wind experiments only, we used principal component analysis (PCA) to create a model for drag moment that resolved collinearity between explanatory variables. The variables included in the analysis were height, stem E, frontal area, volume, mass, number of leaves, stem diameter, and wind velocity. Wind velocity was included due to its variation between individual plants even within the same simulated conditions. Principal component regression was performed on the first two principal components and drag moment from the experiments of the strongest conditions. PCA was not performed on run-up experiments due to there being too few replicates, as stated previously.

For drag coefficient analysis, we statistically regressed the calculated drag coefficient against *Re* and the goodness-of-fit was determined using R^2, and significance, with the p value.

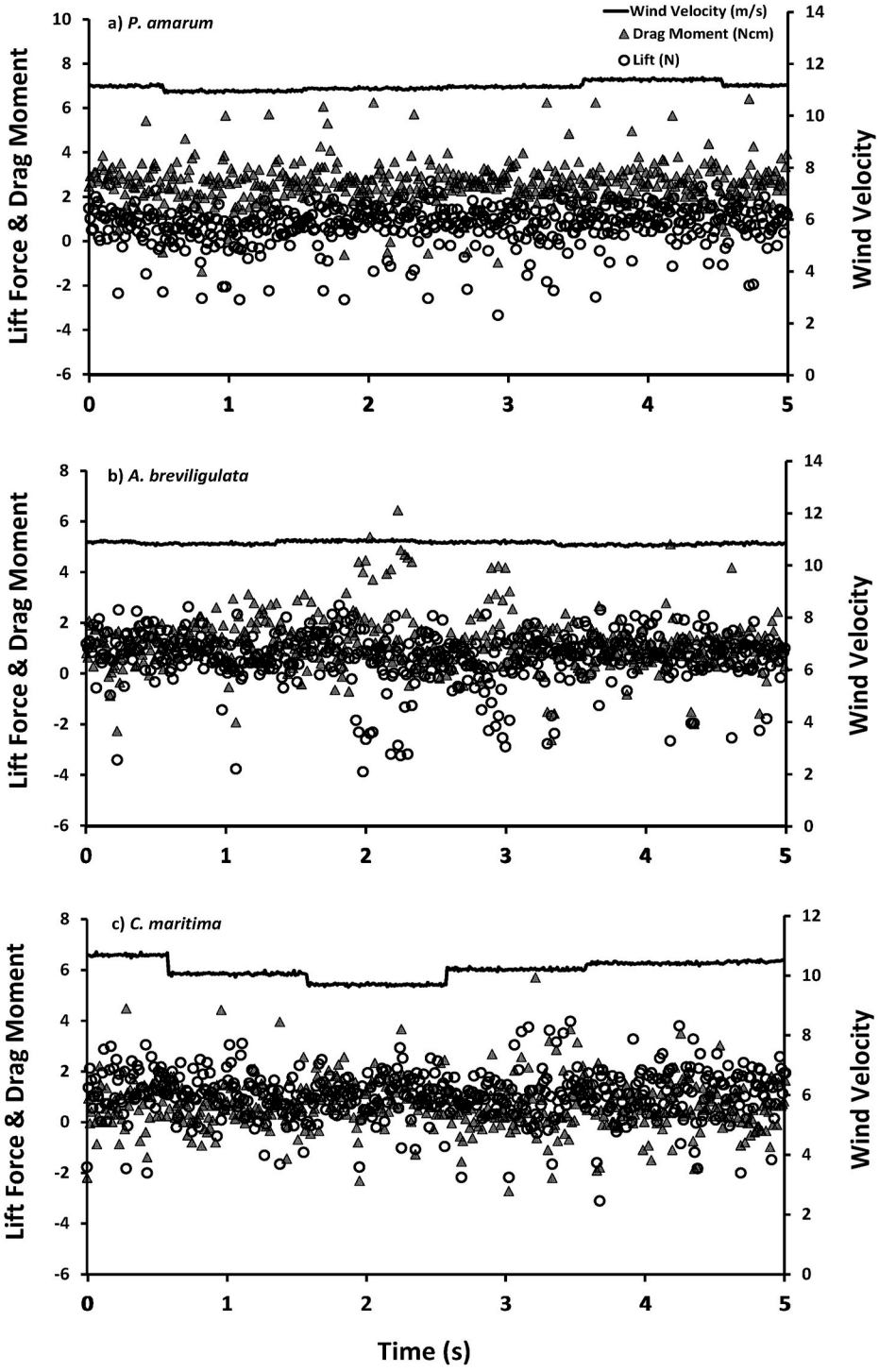

Fig. 3. Time series data for one plant at the greatest wind velocity treatment for (a) *P. amarum*, (b) *A. breviligulata*, and (c) *C. maritima* showed constant lift force and drag moment throughout the trial.

3. Results

Lift force and drag moment plotted over time showed temporal differences in the effects of wind versus run-up energy on the tested plants. Linear regression of force and moment with fluid velocity, run-up water depth, and *Re* related plant response and flow properties. Stepwise multiple regression indicated the most important plant traits for drag moment from wind and run-up experiments. Finally, drag coefficient estimates showed that plant induced drag effects changed with flow turbulence.

3.1. Wind versus run-up forces and moments

Wind and run-up experiments showed different patterns in lift force and drag moment on plants over time. For wind experiments, lift and drag moment for all three species remained relatively constant over time, aside from small variations that did not appear to be directly caused by the wind (Fig. 3). In opposition, run-up displayed a time-dependent relationship between force and the arrival and passing of a run-up event (Fig. 4). The beginning, middle, and end of a run-up event was accompanied by a sharp increase in drag moment and decrease in lift force, a stabilization of both, and finally a decrease in drag moment, respectively. This relationship was seen across all species but was most obvious with *C. maritima* (Fig. 4c).

3.2. Forces and moments related to flow properties

For wind experiments, plants showed greater physical response with increasing wind velocity across all species. Fig. 5 shows measured (a) drag moment and (b) lift force plotted against wind velocity to illustrate this relationship for *A. breviligulata* (AB), *P. amarum* (PA) and *C. maritima* (CM). However, the variation of data points was not constant across velocity (as determined by multiple Barlett's tests), and thus, data was log transformed for linear regression analysis. The physical responses of *P. amarum* and *A. breviligulata* to wind energy were strongly correlated with flow velocity (*P. amarum*: drag moment $R^2 = 0.68$, $p < 0.001$ and lift force $R^2 = 0.33$, $p < 0.001$; *A. breviligulata*: drag moment $R^2 = 0.83$, $p < 0.001$ and lift force $R^2 = 0.43$, $p < 0.001$). For *C. maritima*, these relationships were comparatively weaker (drag moment $R^2 = 0.40$, $p < 0.001$ and lift force $R^2 = 0.14$, $p = 0.007$).

For run-up experiments in general, the forces and moments felt by plants were not well-correlated with the measured water velocity. Instead, plant response was related to run-up water level. Fig. 6 shows each of the tested plants plotted separately, with *A. arenaria* replacing *A. breviligulata* for these experiments (AA; see *Methods* section *Plant biophysical traits*). Linear regression was performed on each species, by combining data from the two plants per species. The drag moment showed no relationship with increasing forward moving velocity for *P. amarum* and *A. arenaria* (Fig. 6a; *P. amarum*: $R^2 = 0.01$, $p = 0.700$; *A. arenaria*: $R^2 = 0.11$, $p = 0.114$), though it was somewhat negatively correlated with velocity for *C. maritima* ($R^2 = 0.31$, $p = 0.014$). On the other hand, drag moment was positively correlated with run-up water level for all species (Fig. 6b). This effect was greatest for *C. maritima* ($R^2 = 0.62$, $p < 0.001$), and less so for *P. amarum* ($R^2 = 0.43$, $p < 0.001$) and *A. arenaria* ($R^2 = 0.28$, $p = 0.007$). There were no significant relationships for lift force and velocity (*P. amarum*: $R^2 = 0.05$, $p = 0.202$; *A. arenaria*: $R^2 = 0.12$, $p = 0.086$; *C. maritima*: $R^2 = 0.16$, $p = 0.088$), nor lift force and water level (*P. amarum*: $R^2 = 0.03$, $p = 0.766$; *A. arenaria*: $R^2 < 0.01$, $p = 0.976$; *C. maritima*: $R^2 = 0.04$, $p = 0.432$).

Plant response was similarly related to flow turbulence (*Re*) as velocity for both wind and run-up experiments. All wind and water flow was categorized as turbulent. In Fig. 7, 'AB/AA' indicates either (a and b) *A. arenaria* in the wind tests or (c and d) *A. breviligulata* in the run-up tests. For wind experiments, drag moment was positively correlated with *Re* for all species (Fig. 7a), with the greatest effect for *A. breviligulata* ($R^2 = 0.77$, $p < 0.001$). This relationship was less strong

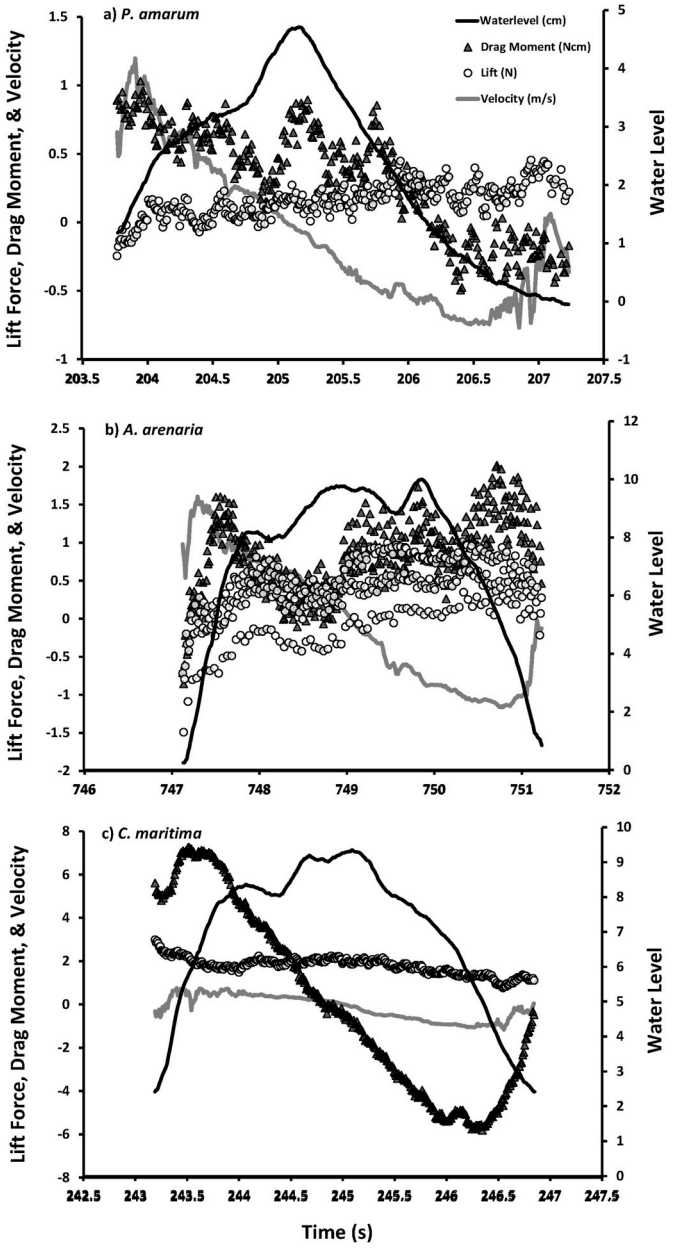

Fig. 4. Lift force and drag moment change with water level and velocity for a single run-up event as run-up initially passes over and washes back for (a) *P. amarum*, (b) *A. arenaria*, and (c) *C. maritima*.

for *P. amarum* ($R^2 = 0.61$, $p < 0.001$) and *C. maritima* ($R^2 = 0.33$, $p < 0.001$). For wind experiments, lift was also significantly correlated with *Re* (Fig. 7b), with *A. breviligulata* showing the strongest relationship ($R^2 = 0.43$, $p < 0.001$), followed by *P. amarum* ($R^2 = 0.31$, $p < 0.001$) and *C. maritima* ($R^2 = 0.13$, $p = 0.008$). For run-up experiments, there were no significant relationship between plant response and *Re* (Fig. 7c, drag moment: *P. amarum*: $R^2 < 0.01$, $p = 0.346$; *A. arenaria*: $R^2 = 0.07$, $p = 0.114$; *C. maritima*: $R^2 = 0.60$, $p = 0.014$; Fig. 7d, lift force: *P. amarum*: $R^2 < 0.01$, $p = 0.966$; *A. arenaria*: $R^2 = 0.08$, $p = 0.086$; *C. maritima*: $R^2 = 0.11$, $p = 0.088$).

3.3. Forces and moments related to plant traits

Plant response to wind was related to several plant biophysical traits (Table 3). For *A. breviligulata*, drag moment was correlated with height ($R^2 = 0.46$, $p = 0.02$) and volume ($R^2 = 0.36$, $p = 0.04$). For *P. amarum*,

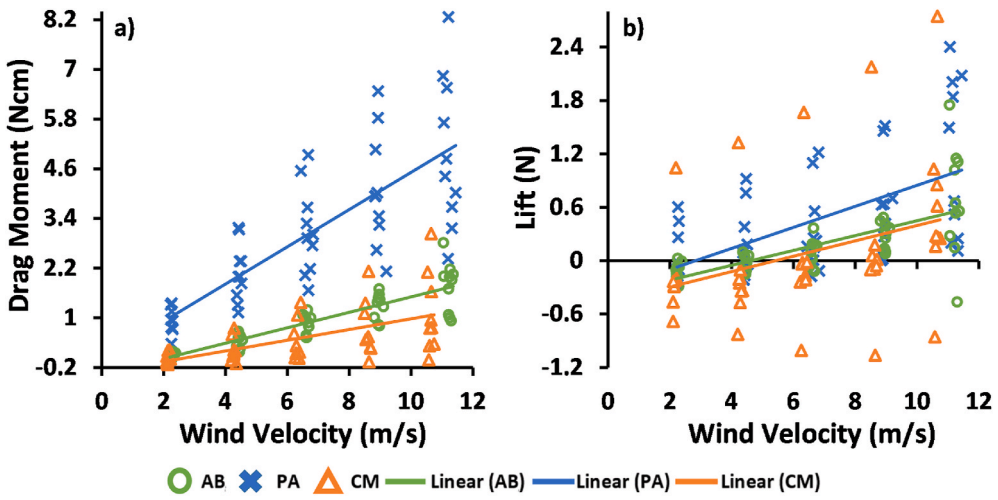

Fig. 5. Plots of (a) drag moment and (b) lift force measured for 50 wind experiments per species. Moment and force increase with wind velocity for *A. breviligulata*, *P. amarum*, and *C. maritima*.

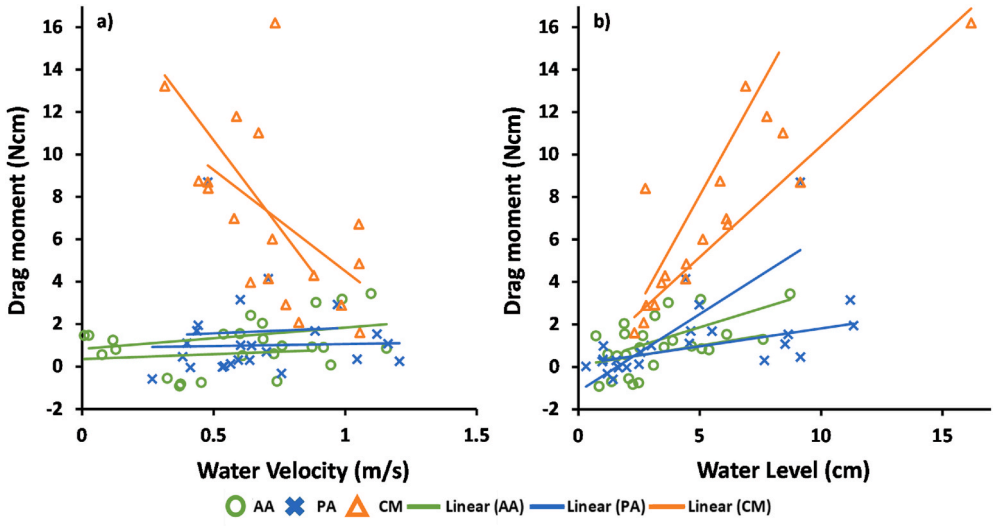

Fig. 6. Plots of (a) drag moment and (b) lift force for 2 plants per species. Moment and force decreased with water velocity for *C. maritima* and increased with water level for *A. arenaria*, *P. amarum*, and *C. maritima*.

drag moment was related to plant height, stem diameter, volume, log function of the number of leaves, and mass, with mass having the greatest effect ($R^2 = 0.70$, $p = 0.002$). None of the biophysical properties included in our study were significantly related to drag moment for *C. maritima*. Additionally, across all species, drag moment was significantly correlated with the following biophysical traits: plant height ($R^2 = 0.764$ $p < 0.001$), function of the number of leaves ($R^2 = 0.12$, $p = 0.039$), function of the stem E ($R^2 = 0.39$, $p < 0.001$), and frontal area ($R^2 = 0.15$, $p = 0.022$).

Importantly, we included wind velocity (or run-up water level for run-up tests) as an independent variable in our regression analyses. This allowed us to identify whether differing experimental conditions had an effect on the forces and moments felt by the plants. For wind experiments, the drag moment was weakly correlated with wind velocity ($R^2 = 0.11$, $p = 0.043$) when all species were combined. To follow up, we tested for significant differences among the wind velocities for each species using ANOVA. This analysis showed that the conditions experienced by the relatively short *C. maritima* were significantly different from *A. breviligulata* and *P. amarum* at each trial ($p < 0.001$), though the latter two were not significantly different from one another.

Finally, stepwise multiple regression showed that the optimal predictive model for wind-induced drag moment on dune plants included plant height and wind velocity ($R^2 = 0.80$, $p < 0.001$). Wind induced lift was not significantly correlated with any independent variables from simple linear regression (see Supplemental Table I) or stepwise multiple regression.

Plant response to run-up for all species combined was correlated with plant height ($R^2 = 0.63$, $p = 0.041$), number of leaves ($R^2 = 0.67$, $p = 0.033$), and mass ($R^2 = 0.66$, $p = 0.028$; Table 4). We were not able to analyze each species individually for run-up experiments due to a lack of replicates (see *Methods* section Table 1). Additionally, stepwise multiple regression only included number of leaves ($R^2 = 0.67$, $p = 0.030$) as the most important explanatory variable for run-up induced drag moment. Lift was not correlated with any of the biophysical variables for run-up experiments (see Supplemental Table II).

PCA was also performed on wind induced drag moment from the greatest test conditions. The first two principle components (PC1 and PC2) described approximately 41% and 34% of variation in explanatory variables, respectively (see Supplemental Figure VI). PC1 was positively correlated with plant mass and number of leaves, and negatively correlated with wind velocity, indicating PC1encompassed the biophysical variation between the graminoid species (*A. breviligulata* and

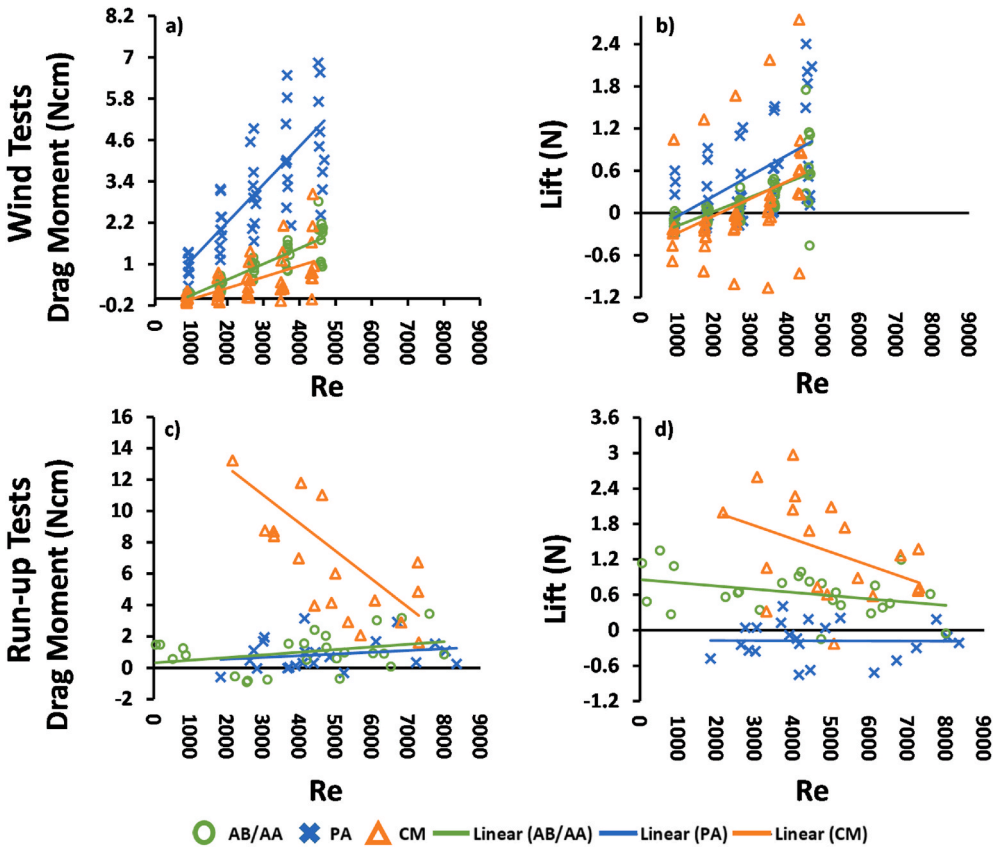

Fig. 7. Reynolds number was positively related to (a) wind induced drag moment and (b) wind induced lift force, but not related to (c) run-up induced drag moment, nor (d) run-up induced lift force.

Table 3
Linear regression analysis results* for wind induced drag moment and plant traits for each species individually and all species combined. Stepwise multiple regression results for wind induced drag moment and plant traits of all species combined.

Wind Drag Moment and Plant Traits - Simple Linear Regression								
	Combined		*A. breviligulata*		*C. maritima*		*P. amarum*	
	Adj. R^2	p-value	Adj. R^2	p-value	Adj. R^2	p-value	Adj. R^2	p-value
Height	0.64	<0.001	0.46	0.019	0.004	0.343	0.54	0.009
Stem diameter	-0.01	0.433	023	0.093	-0.10	0.629	0.66	0.003
Volume	0.06	0.112	0.36	0.038	-0.13	0.668	0.35	0.036
Log(# of leaves)	0.12	0.039	0.24	0.088	-0.07	0.522	0.60	0.006
Log(stem E Estimate)	0.39	<0.001	-0.12	0.911	-0.07	0.481	0.04	0.271
Mass	0.02	0.240	-0.11	0.729	-0.13	0.767	0.70	0.002
Frontal area	0.15	0.022	-0.03	0.423	-0.13	0.783	0.18	0.142
Wind velocity	0.11	0.043	0.06	0.254	-0.06	0.471	0.12	0.170
Wind Drag Moment and Plant Traits - Stepwise Multiple Regression								
	Combined Adj. R^2	p-value	Notes					
height	0.64	<0.001	Height alone accounts for 64% of the variance in drag moment between plants.					
+Wind velocity	0.80	<0.001	Knowledge of wind velocity increases R^2 by 0.16 beyond knowledge of height alone.					

* R^2 and associated significance p values from linear regressions of plant characteristic and drag moment measured at the greatest wind velocity.

Significant correlations are shaded ($p \leq 0.05$). Negative R^2 values indicate non-significant explanatory variables.

P. amarum) and *C. maritima*. PC2 was most closely related to frontal area, volume, and stem E, and inversely related to stem diameter (see Supplemental Figure VII), making it representative of the variation between the graminoid species. Linear regression of PC1 and drag moment showed a negative relationship; however, the correlation was weak and not significant ($R^2 = 0.05$, $p = 0.14$). In contrast, PC2 was positively correlated with drag moment in a strong and significant manner (Supplemental Figure VIII, $R^2 = 0.37$, $p < 0.001$).

Table 4
Linear regression analysis results* for run-up induced drag moment and plant traits for all species combined. Stepwise multiple regression results for run-up induced drag moment and plant traits of all species combined.

Run-up Drag Moment and Plant Traits - Simple Linear Regression		
	Combined	
	Adj. R^2	p-value
Height	0.63	0.041
Stem diameter	-0.12	0.525
# of leaves	0.67	0.033
Log(stem E Estimate)	0.11	0.279
Mass	0.66	0.028
Frontal area	0.31	0.154
Water velocity	-0.25	0.921
Water level	-0.16	0.609

Run-up Drag Moment and Plant Traits - Stepwise Multiple Regression			
	Adj. R^2	p-value	Notes
# of leaves	0.67	0.030	Number of leaves alone accounts for 67% of the variance in drag moment between plants.

* R^2 and associated significance p values from linear regressions of plant characteristic and drag moment measured at the greatest run-up water depth. Significant correlations are shaded ($p \leq 0.05$). Negative R^2 values indicate non-significant explanatory variables.

3.4. Drag coefficient analysis

The plants affected flow differently with increasing flow turbulence, as expected. Plant drag coefficients for wind ranged from 5.0×10^{-4} to 3.6×10^{-2}, and for run-up ranged from 2.7×10^{-3} to 1.7. While other studies have shown non-linear relationships between C_D and *Re* (Vuik et al., 2016), a linear equation was the best fit for our experiment. In general, there was a negative relationship between the C_D of the plant and *Re* (Fig. 8) for both (a) wind and (b) run-up experiments. The exception to this pattern was *C. maritima*, which had an increasing drag effect with *Re* for wind experiments. Linear regression analysis showed C_D was significantly correlated with *Re* for *P. amarum* wind experiments ($R^2 = 0.48$ $p < 0.001$) and for *C. maritima* ($R^2 = 0.33$, $p = 0.010$) and *A. arenaria* ($R^2 = 0.54$, $p < 0.001$) run-up experiments. Finally, C_D was significantly correlated with *Re* for run-up experiments for all species combined ($R^2 = 0.27$, $p < 0.001$), but not for wind ($R^2 < 0.01$, $p = 0.738$).

4. Discussion

Coastal dune plants experienced very different physical pressures from wind versus water energy. The results of our experiments showed a complex relationship between flow properties, plant traits, and plant response. The drag moments and lift forces a plant experienced from wind versus run-up were affected by different flow properties and plant biophysical traits. Moreover, the drag coefficient estimates showed that plants affected flow differently at harsher flow conditions. These vegetation parameters can be used to improve process-based coastal models, such as XBeach (Roelvink et al., 2009) and COAWST (Warner et al., 2010).

4.1. Wind versus run-up forces and moments

Plants experienced different forces over time, depending on whether they were affected by wind or run-up energy. Our experiments showed that wind delivered relatively constant mean forces and moments over time, whereas run-up induced changing forces, strongly tied to the arrival and backwash of individual run-up bores. The plants also felt different magnitudes of forces and moments from wind versus run-up. This was especially true in terms of the drag moment, in which run-up had a much greater effect on plants (producing a peak drag moment of 20 Ncm). Our results suggest, under field conditions during storms or unusually high tide events, plants on the dune toe and back beach can experience relatively low, constant forces and moments from wind, while at the same time, be more forcefully moved landward and up, then seaward and down by the intercepting run-up waves.

4.2. Fluid flow properties and exerted forces

The physical effects of wind and run-up energy on dune plants were influenced differently by flow properties, as expected. Wind and wave run-up conditions are varied in terms of fluid density, flow structure, boundary layer interactions, and inertial versus drag effects. From our experiments, fluid density emerged as the strongest physical factor differentiating wind versus run-up effects on plants. Initially, the greater magnitude of run-up induced drag moment (discussed in the previous paragraph) was interesting given that run-up often only affected the lower portion of the plant, while wind affected the entire plant. However, linear regression analysis for run-up experiments showed drag moment was strongly correlated with water level, but not water velocity. This suggests that, while flow velocity was necessary to induce a drag moment, the greater fluid density of water relative to air was key for the differences between wind versus run-up induced plant response.

Another explanation for the observed difference in drag moment magnitudes could come from the integration of a series of horizontal forces over the vertical dimension, each with different velocities, cross-sectional areas, drag, etc. - similar to the Morison equation (Equation (4)). In the case of wind, fine-scale spatial and temporal oscillations may cancel themselves across the vertical dimension, leading to a lower net value. For run-up, these oscillations would occur at a much larger time scale. Plant flexibility would add further complexity, since all these parameters would depend on the bending of each species (i.e., stem E). These ideas might be further explored by relating drag moment with another descriptor of wave propagation, such as energy and/or power.

As previously mentioned, velocity was variably related to drag moment and lift force on plants. Whereas wind experiments showed a strong and significant relationship between velocity and drag moment and lift force, run-up experiments did not. This lack of relationship can be explained by considering the different aspects of the run-up flow. Run-up is formed from waves breaking in the swash zone and reforming

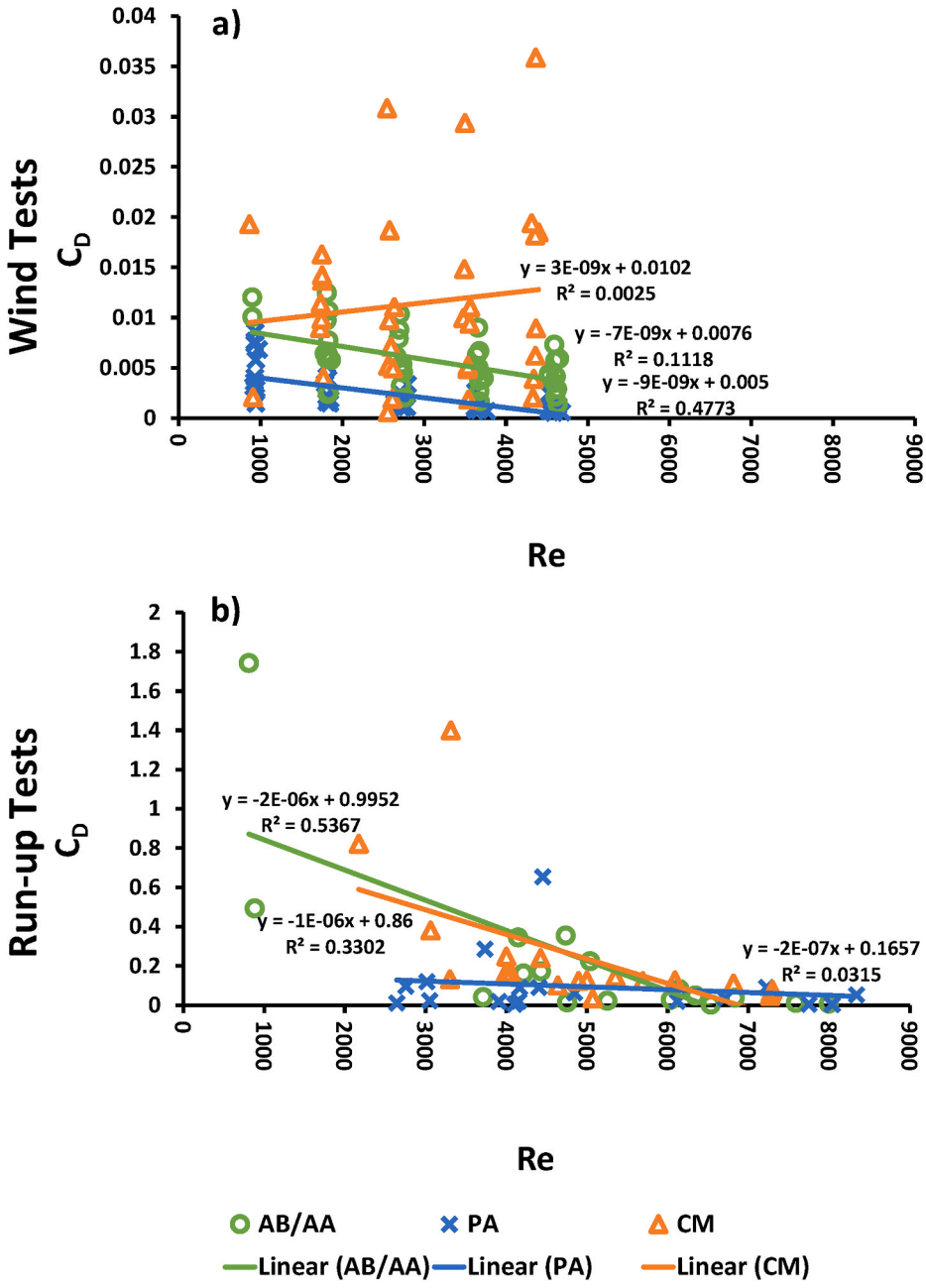

Fig. 8. C_D decreases across turbulence conditions for (a) wind and (b) run-up experiments.

in accordance with depth limitations, until water is forced up the beach slope as a run-up bore. As a result, the water velocity at a single point within a bore (as we measured using the Vectrino) is constantly changing. A bore-intercepted plant is then likely affected differently throughout the water column, causing a dissociation between the plant's response and a point velocity measurement. Pairing a plant's response to run-up with water velocity recorded over a range of water depth, such as measured by a Vectrino Profiler (Nortek, Inc.), could test this idea. Finally, *Re* was similarly related to lift force and drag moment due to the direct relationship with velocity (see Equation (2)).

Future studies could expand on our research by exploring the specific mechanisms of wind and run-up effects on plants - especially lift force. One possible source might be the deformation of the vegetation: a bending plant stem could cause a pulling force that is consequently interpreted as lift. An experiment that measured the proportionality of lift to flow velocity, drag, and the Young's Modulus (E) could test this hypotheses. Alternatively, lift force specifically from run-up experiments could be due to a "Bernoulli" effect, where the stagnant velocity inside the sand may induce a vertical pressure gradient (Bernoulli, 1738). In this case, lift would be proportional to the square of the velocity and fluid density. Plant buoyancy could also contribute to run-up induced lift, which could be accounted for in future studies by measuring the mass of water displaced by the plant stem and plotting it beside lift over time.

Moreover, run-up induced drag moment and drag coefficient estimations could be improved by accounting for inertial forces in the Morison equation (Equation (4)). For unsteady flows such as in our run-up experiments, calculation of the total force incorporates inertial force and drag force:

$$F = \rho C_m V \dot{U} + \frac{1}{2}\rho C_D A U^2 \quad (5)$$

The inertial force (first half of right side of equation) is a product of

the fluid density (ρ), an inertia coefficient (C_m), plant volume (V), and flow acceleration ($\mathring{U}$) and can be comparable to the drag force in magnitude. However, inertial force was not accounted for in our run-up experiments as total plant volume was not collected for these tests, and estimating the inertia term would require erroneous assumptions about plant volumes since no true value could be applied. Plant volume could be estimated from the stem diameter and the instantaneous water depth; however, this value would not be accurate, due to the complex architecture of real plants which involves much more than the stem diameter alone - especially when considering *C. maritima* individuals. Moreover, this architecture would need to be considered time-variant according to the level of submergence and subtle interplay between flow and flexibility of shape. Furthermore, our experimental set-up involved exposing plants to run-up bores, which consist of varying flows (in terms of magnitude and direction) throughout the water column at a single instant, and incorporating flow acceleration at a single point (as measured by the Vectrino) into the inertia term estimation would not be representative of all conditions experienced by the plant. As a result, run-up induced drag moment and drag coefficient values from our experiments could be overestimated, as our force sensor measured the total resultant force on the plant, and this force was subsequently used for calculations.

Future work could account for inertial forces by including the inertial term in the Morison equation, or by identifying a range of Keulegan-Carpenter numbers for a given run-up condition. The latter method would describe the relative importance of the drag forces over inertia forces for bluff objects in an oscillatory fluid flow from the amplitude of the flow velocity oscillation, the period of oscillation and a characteristic length (such as stem diameter) (Dean and Dalrymple, 1991). To achieve this goal however, would require the development of new methods of recording instantaneous submerged plant volume. One potential route for such work is to measure the water volume displacement during submergence by recording the water level at an extremely high resolution in a relatively small flume. Even this method would have to account for any underlying dune morphology contribution to water level displacement; clearly new methods are needed to arrive at the inertial term, when moving this area of research beyond the use of a flat bottom and synthetic and simple plant structures. For the wind experiments, the inertial term was less impactful as velocity remained constant for the duration of the experiments.

4.3. Plant biophysical traits and exerted forces

Plant biophysical traits differently influenced wind versus run-up effects in our experiments. For wind experiments, plant height was most important for predicting drag moment. However, the presence of a boundary layer also likely strengthened plant height effects (Supplemental Figure IV), as wind velocity emerged with plant height from stepwise multiple regression. A boundary layer is formed when friction from the bed causes the fluid velocity to slow. In our wind experiments, the boundary layer in the wind tunnel caused shorter plants to experience lower wind velocities. This affect was further supported by an ANOVA test performed on the wind velocities measured at the height of each plant species, which showed that the velocities experienced by *C. maritima* individuals were significantly less than that for both *A. breviligulata* and *P. amarum*. Moreover, principal component regression performed to relate wind induced drag moment to PC1 showed that drag moment was inversely related to PC1. This relationship indicated that drag moment was negatively related to morphological and wind velocity dissimilarities between the graminoid species and *C. maritima* (i.e., the more a plant was like *C. maritima*, the less drag moment it experienced). While the effect of height on drag moment was somewhat complicated by the extent of the boundary layer, this phenomenon is representative of what occurs under field conditions.

Additionally, principal component regression showed wind induced drag moment was strongly and directly related to PC2, which was synonymous with the morphological and wind velocity differences between *A. breviligulata* and *P. amarum* (Supplemental Figure VII). This relationship might be explained by stem structure and boundary layer effects: *P. amarum* plants had greater frontal area above the boundary layer compared to *A. breviligulata* (see Fig. 2). However, plant avoidance also may have contributed to the observed drag moment differences, as stem E was greater for *P. amarum* compared to *A. breviligulata,* indicating less stem flexibility, and thus less propensity to streamline. Furthermore, drag coefficient analysis showed that *A. breviligulata* drag effects decreased faster than those of *P. amarum* at greater wind turbulences, as is consistent with plant streamlining. Future research should include more species of dune grasses in the study, to encompass a larger range of biophysical traits, and explore the relative importance of each in relation to exerted forces.

In contrast to wind experiments, run-up experiments did not show a relationship between plant height and drag moment, probably due to the flow structure within a run-up bore (as previously discussed) and the absence of a developed boundary layer. Instead, the number of leaves was most important for predicting run-up induced drag moment, possibly due to the interactions between flow turbulence and plant structure. We suggest - based on experimental observations - that heterogeneous plant structure may be able to capture more turbulent eddies compared to homogenous or streamlined structure, thereby affecting the energy released into the plant. Since turbulence can also reduce drag in some cases, flow statistics can be considered in future studies to determine the mechanism of run-up induced drag moment.

4.4. Drag coefficient and consequences for management

The drag coefficients (C_D) derived from our study are aligned with those from previous studies when key experimental differences are considered (Table 5). However, our study was unique among them because it: 1) simulated run-up, which has a different flow structure from oscillatory waves and linear flows tested in other studies, 2) tested both submerged and emergent plants, depending on the depth of an individual run-up event, and 3) used real plants, which involves greater complexity (i.e., plant morphology, flexibility, structural integrity, etc.) than commonly used synthetic proxies. C_D encompasses object-specific drag (skin friction and form drag) and is affected by flow conditions, such as velocity and fluid density, and in our experiment all of these values varied instantaneously depending on the level of submergence and plant structural response. As a result, our C_D estimates can only be indirectly compared to those from existing literature.

For instance, Ishikawa et al. (2000) estimated C_D for much larger trees exposed to water flow (velocities from 2.25 m/s – 4.50 m/s) to be 0.5–1, and Kothyari et al. (2009) estimated C_D for unsubmerged rigid vegetation (maximum velocity of 0.24 m/s) to be 0.75–2. Compared to these values, C_D from our run-up experiments (estimated as 2.7×10^{-3} - 1.74 at run-up water velocities <0.1 m/s- 1.21 m/s) seemed much lower. However, both Ishikawa et al. and Kothyari et al. used much stiffer wooden and stainless-steel dowels as proxies for real plants to derive a bulk drag coefficient, which does not represent the drag coefficient of an isolated plant, but rather a bulk drag coefficient that is temporally and spatially averaged over the vegetation patch. The different results seen in our experiments could be due to greater streamlining at lower velocities by actual plants versus plant-substitutes. Alternatively, variations in plant shapes could be responsible for the observed discrepancies, as Thompson et al. (2003) tested isolated plant-substitutes of different geometries under water flow and found C_D ranged from 0.80 to 1.65 solely due to shape variations. Studies that involved actual plants include Butler et al. (2012), which estimated C_D for plants exposed to wind (maximum velocity 30 m/s) to be 0.21–0.46; however, they only considered relatively stiff woody plants. Additionally, a more comparable water study measured water flow effects (0 m/s −20 m/s) on two kelp fronds and estimated drag force to be 0.005–0.02N (Wilson et al., 2008). Although they did not provide C_D

Table 5
Literature-based values for drag coefficients of vegetation exposed to waves or water flow. Studies are ranked by maximum C_D value.

Authors	Year	Target vegetation	C_D	Flow conditions	Structure	Bulk/Individual
Paul and Amos	2011	*Zostera noltii*	0.13	*Re*: 1000	Natural	Bulk
Pinskey et al.	2013	several salt marsh vegetation species	0.14	*Re*: 1000	Natural	Bulk
Moller et al.	2014	predominantly *Elymus athericus*	0.25	*Re*: 1000	Natural	Bulk
Vuik et al.	2016	*Spartina anglica* and *Scirpus maritimus*	0.4–0.6	*Re*: 400–1200	-	Bulk
Devi and Kumar	2016	*Oryza sativa*	0.468–0.692	Velocity: 0.1–0.4 m/s	Mimic	Bulk
Wunder et al.	2011	*Salix viminalis, Salix alba*, and *Salix purpurea*	0.3–1.0	Velocity: 0.3–0.7 m/s	Natural	Individual
Augustin et al.	2009	*Spartina alterniflora*	0.1–1.1	*Re*: 3500-8500	Mimic	Bulk
Hu et al.	2014	-	1.69	*Re*: 1000	Mimic	Bulk
Innocenti et al. (this study)	-	*A. arenaria*, *A. breviligulata*, *C. maritima*, and *P. amarum*	0.0027–1.74	*Re*: 811–8340 Velocity: <0.12–1.21 m/s	Natural	Individual
Anderson and Smith	2014	*Spartina alterniflora*	1.0–2.5	*Re*: 500 - 2250	Mimic	Bulk
Peruzzo et al.	2018	*Spartina maritima*	0.2–3.2	*Re*: 50 - 850	Mimic	Bulk
Jadhav	2012	*Spartina alterniflora* and *Spartina patens*	1.2–4.3	*Re*: 500 - 3500	Natural	Bulk
Mendez et al.	1999	-	5.75	*Re*: 1000	Mimic	Bulk
Vanegas et al.	2019	*Rhizophora mangle*	0.8–8.0	*Re*: 3.0×10^5–8.0×10^5	Nnatural	-
Cantalice et al.	2015	*Ipomoea pes-caprae*	0.050–19.861	Velocity: 0.095–0.295 m/s	Natural	Bulk

estimates, it is apparent that kelp is extremely flexible and soft and this lowers the drag force.

The drag coefficients from our study can be used by coastal managers as parameters for coastal models such as XBeach (Roelvink et al., 2009). Besides the drag coefficients we provide for three species of dune plants, those for other dune species can be estimated using Fig. 8. To do this, first, the physical structure of the species must be determined. A visual description of height, leaf and branch structure, and frontal area would be sufficient, or species traits could be compared from the data published in Feagin et al. (2019). Then, the species of interest must be categorized into likeness of a species from our experiments. Finally, the modeled flow turbulence must be input to the corresponding regression line from Fig. 8 to calculate the drag coefficient.

For example, to find the drag coefficient of *Spartina patens* (*S. patens*) under run-up conditions, the modeler could assess the species to most resemble *A. arenaria*, due to its tall, thin structure. Then, the C_D could be calculated using the modeled run-up *Re* and the *A. arenaria* run-up regression line from Fig. 8:

$$C_D = -2 \times 10^{-6}(Re) + 0.9952 \quad (6)$$

On the other hand, a species such as *Ipomoea pes-capre* that is shorter, with many, large leaves, would better resemble *C. maritima*. In this case, the trend line of *C. maritima* would be utilized for drag coefficient estimation. Alternatively, assessing species likeness can be skipped by averaging all the trend lines from Fig. 8 to create a general equation for drag coefficient. However, ignoring species-specific traits adds a greater degree of error to the estimation. These C_D estimates can be incorporated into coastal models as opposed to a constant value to calculate species-specific damping in the fluid field by vegetation.

4.5. Dune plant strategies against wind and run-up forces

In coastal ecosystems, natural and anthropogenic disturbances can alter successional trajectories on dunes (Feagin et al., 2015). Dune plant physiognomy and spatial arrangement on the dunes are likely related to their ability to tolerate or avoid these forces (Feagin et al., 2019). Taller dune grasses such as *P. amarum*, *A. brevigulata*, and *A. arenaria*, often grow on the tops of dunes, at locations that have relatively high wind velocities but rarely experience run-up. Their height will allow greater interaction with wind energy, and affect wind flow carrying sand. Sand deposition leads to plant burial, which stimulates growth and further dune development (Maun, 1998; Duran and Moore, 2013). These conditions cause a positive feedback loop, and build taller dunes to allow these species to persist at more habitable conditions on the tops of dunes.

In contrast, short plants, including succulents like *C. maritima*, often grow on the back beach or on embryonic dunes, where they are subject to more wave run-up, but relatively less wind compared to plants on dune crests, due to their height and the presence of a boundary layer. The leaves and dense biophysical structure of these plants will more strongly interact with run-up energy, and, as we observed in our experiments, this type of disturbance can cause pieces of vegetative material to break and float offshore. Consequently, many of these species have low seed viability, and instead reproduce vegetatively via deposition of these broken-off shoots and rhizomes (Feagin et al., 2015).

In the context of restoration goals, our findings can be implemented in the field by ensuring restored dunes are vegetated with a diverse range of species, common to all locations of the dunes. Our study shows dune species interact differently with erosive wind or run-up forces depending on the flow conditions and species' biophysical traits. These factors also influence how effective plants are at inducing drag on wind and run-up energy, and consequently, sediment transport. Managers can strategically place species of dune plants to capitalize on their energy-reducing qualities, based on whether the plant is adapted to conditions more common to the dune crest or dune toe. Tall, thin dune grasses should be planted on the dune crest and dune fronts due to their ability to mitigate wind energy. Conversely, low shrubby plants should be planted on the dune toe because of their resiliency to run-up energy. By maintaining biodiversity on the coast, managers can better equip these areas to resist erosive forces and to naturally rebuild after disturbance.

5. Conclusions

This study clarified the forces and moments imposed on dune plants during disturbance from wind and wave run-up, and related plant response to flow properties and plant traits. Wind induced drag moment was significantly related to wind velocity for all species (*P. amarum* $R^2 = 0.68$, $p < 0.001$; *A. breviligulata* $R^2 = 0.83$, $p < 0.001$; *C. maritima*, $R^2 = 0.40$, $p < 0.001$) whereas run-up induced drag moment was related to water level (*P. amarum* $R^2 = 0.43$, $p < 0.001$; *A. arenaria* $R^2 = 0.28$, $p = 0.007$; *C. maritima* $R^2 = 0.62$, $p < 0.001$), probably due to the turbulence within the run-up bores affecting plants differently throughout the water column. These results suggest that fluid density was the strongest physical factor determining the difference between wind versus run-up effects on plants. Additionally, wind-induced forces and moments were most dependent on plant height ($R^2 = 0.64$, $p < 0.001$), the effect of which was likely strengthened by the presence of a boundary layer causing lesser conditions on plants shorter than 20 cm. Alternatively, forces and moments due to run-up were influenced by plant number of leaves ($R^2 = 0.67$, $p = 0.030$), likely due to plant heterogeneity capturing turbulent eddies which in turn transferred energy down the plant stem. Drag coefficient estimates for each species ranged from 5.0

$\times 10^{-4}$ to 3.6×10^{-2} for wind experiments and 2.7×10^{-3} to 1.7 for run-up experiments, and were only weakly related to Reynolds number for *P. amarum* wind tests ($R^2 = 0.47$ $p < 0.001$) and *C. maritima* run-up tests ($R^2 = 0.29$ $p < 0.010$). This data provides valuable information on the benefits of dune vegetation to interrupting flow by inducing drag, such that modelers and managers can better understand how to best protect coastlines.

Author statement

Rachel A. Innocenti: project administrator, conceptualization, methodology, software, formal analysis, investigation, data curation, writing - original draft, writing – review & editing, visualization.

Rusty A. Feagin: supervision, conceptualization, methodology, validation, resources, writing - original draft, writing – review & editing, funding acquisition.

Bianca R. Charbonneau: methodology, investigation, writing - original draft, writing – review & editing, visualization, resources.

Jens Figlus: supervision, conceptualization, validation, resources, writing – original draft.

Pedro Lomonaco: conceptualization, validation, resources, investigation, writing – original draft, funding acquisition.

Meagan Wengrove: investigation, validation, conceptualization, resources, writing – original draft, supervision, funding acquisition.

Jack Puleo: investigation, validation, conceptualization, resources, writing – original draft, supervision, funding acquisition.

Thomas P. Huff: investigation, methodology, conceptualization, software, validation, writing - original draft.

Yashar Rafati: conceptualization, methodology, investigation, validation, writing - original draft.

Tian-Jian Hsu: validation, writing - original draft, funding acquisition.

Maria V. Moragues: conceptualization, writing – original draft, writing – review and editing, visualization.

Benjamin Tsai: validation, writing – original draft, investigation.

Thomas Boutton: validation, conceptualization, writing – original draft.

Maria Pontiki: investigation, conceptualization, writing – original draft.

Jeremy Smith: investigation, conceptualization, writing – original draft.

Declaration of competing interest

The authors declare that they have no known competing financial interests or personal relationships that could have appeared to influence the work reported in this paper.

Acknowledgements

This research was funded by NSF-OCE (projects #1756449, 1756477, 1756714), NSF-CMMI-NHERI (project #1519679), DOD-NDSEG (project #FA9550-11-C-0028), and USACE-ERDC/USGS.

Appendix A. Supplementary data

Supplementary data to this article can be found online at https://doi.org/10.1016/j.ecss.2021.107556.

References

Albayrak, I., Nikora, V., Miler, O., O'Hare, M., 2012. Flow-plant interactions at a leaf scale: effects of leaf shape, serration, roughness and flexural rigidity. Aquat. Sci. 74 (2), 267–286.

Anderson, M.E., Smith, J.M., 2014. Wave attenuation by flexible, idealized salt marsh vegetation. Coast Eng. 83 (1), 82–92.

Augustin, L.N., Irish, J.L., Lynett, P., 2009. Lab and numerical studies of wave damping by emergent and near-emergent wetland vegetation. Coast Eng. 56 (3), 332–340.

Barbier, E.B., Hacker, S.D., Kennedy, C., Koch, E.W., Stier, A.C., Silliman, B.R., 2011. The value of estuarine and coastal ecosystem services. Ecol. Monogr. 81 (2), 169–193.

Baron-Hyppolite, C., Lashley, C.H., Garzon, J., Miesse, T., Ferreira, C., Bricker, J.D., 2019. Comparison of implicit and explicit vegetation representations in SWAN hindcasting wave dissipation by coastal wetlands in chesapeake bay, 2076-3263 Geosciences 9 (1), 8–1.

Bernoulli, D., 1738. Hydrodynamica, sive de viribus et motibus fluidorum commentarii: opus academicum ab auctore, dum Petropoli ageret, congestum. sumptibus Johannis Reinholdi Dulseckeri, Argentorati.

Borisevich, S.A., Vikhrenko, V., 2018. Evaluation of the drag coefficients of tree crowns by numerical modeling of their free fall. Agric. For. Meteorol. 256, 346–352.

Bouws, E., Günther, H., Rosenthal, W., Vincent, C.L., 1985. Similarity of the wind wave spectrum in finite depth water: 1. Spectral form. J. Geophys. Res. 90 (C1), 975–986.

Butler, D.W., Gleason, S.M., Davidson, I., Onoda, Y., Westoby, M., 2012. Safety and streamlining of woody shoots in wind: an empirical study across 39 species in tropical Australia. New Phytol. 193, 137–149.

Cantalice, J.R.B., Melo, R.O., Silva, Y.J.A.B., Cunha Filho, M., Araújo, A.M., Vieira, L.P., Bezerra, S.A., Barros Jr., G., Singh, V.P., 2015. Hydraulic roughness due to submerged, emergent and flexible natural vegetation in a semiarid alluvial channel. J. Arid Environ. 114, 1–7.

Cao, J., Tamura, Y., Yoshida, A., 2012. Wind tunnel study on aerodynamic characteristics of shrubby specimens of three tree species. Urban For. Urban Green. 11 (4), 465–476.

Charbonneau, B.R., 2015. A review of dunes in today's society. Coast. Manag. 43, 465–470.

Chen, H., Zou, Q.-P., 2019. Eulerian-Lagrangian flow-vegetation interaction model using immersed boundary method and OpenFOAM. Adv. Water Resour. 126, 176–192.

Dean, R.G., Dalrymple, R.A., 1991. Water Wave Mechanics for Engineers and Scientists. World Scientific, Singapore.

Devi, T.H., Kumar, B., 2016. Flow characteristics in an alluvial channel covered partially with submerged vegetation. Ecol. Eng. 94, 478–492.

Duran, O., Moore, L.J., 2013. Vegetation controls on the maximum size of coastal dunes. Proc. Natl. Acad. Sci. U.S.A. 110 (43), 17217–17222.

Elko, N., Brodie, K., Stockdon, H., Nordstrom, K., 2016. Dune management challenges on developed coasts. Shore Beach 84, 15–28.

Everard, M., Laurence, J., Watts, B., 2010. Have we neglected the societal importance of sand dunes?. An ecosystem services perspective. Aquat. Conserv. Mar. Freshw. Ecosyst. 20, 476–487.

Fang, J., Peringer, A., Stupariu, M., Patru-Stupariu, I., Buttler, A., Golay, F., Porte-Agel, F., 2018. Shifts in wind energy potential following land-use driven vegetation dynamics in complex terrain. Sci. Total Environ. 639, 374–384.

Feagin, R.A., Lozada-Bernard, S.M., Ravens, T.M., Möller, I., Yeager, K.M., Baird, A.H., 2009. Does vegetation prevent wave erosion of salt marsh edges? Proc. Natl. Acad. Sci. U.S.A. 106 (25), 10109–10113.

Feagin, R.A., Irish, J.L., Moller, I., Williams, A.M., Colon-Rivera, R.J., Mousavi, M.E., 2011. Short communication: engineering properties of wetland plants with application to wave attenuation. Coast Eng. 58, 251–255.

Feagin, R.A., Figlus, J., Zinnert, J.C., Sigren, J., Martínez, M.L., Silva, R., Smith, W.K., Cox, D., Young, D.R., Carter, G., 2015. Going with the flow or against the grain? The promise of vegetation for protecting beaches, dunes, and barrier islands from erosion. Front. Ecol. Environ. 13 (4), 203–210.

Feagin, R.A., Furman, M., Salgado, K., Martinez, M.L., Innocenti, R.A., Eubanks, K., Figlus, J., Huff, T.P., Sigren, J., Silva, R., 2019. The role of beach and sand dune vegetation in mediating wave run up erosion. Estuarine. Coastal and Shelf Science 219, 97–106.

French, P.W., 2001. Coastal Defenses: Processes, Problems and Solutions. Routledge, London.

Gijón Mancheño, A., Jansen, W., Winterwerp, J.C., Uijttewaal, W.S.J., 2021. Predictive model of bulk drag coefficient for a nature-based structure exposed to currents. Sci. Rep. 11 (1), 3517.

Harman, B.P., Heyenga, S., Taylor, B.M., Fletcher, C.S., 2015. Global lessons for adapting coastal communities to protect against storm surge inundation. J. Coast Res. 31 (4), 790–801.

Hesp, P.A., 2013. Conceptual Models of the evolution of transgressive dune field systems. Geomorphology 199, 138–149.

Hijuelos, A.C., Dijkstra, J.T., Carruthers, T.J.B., Heynert, K., Reed, D.J., van Wesenbeeck, B.K., 2019. Linking management planning for coastal wetlands to potential future wave attenuation under a range of relative sea-level rise scenarios. PloS One 14 (5), 1–19.

Hu, Z., Suzuki, T., Zitman, T., Uijttewaal, W., Stive, M., 2014. Laboratory study on wave dissipation by vegetation in combined current-wave flow. Coast Eng. 88, 131–142.

Huang, Z., Yao, Y., Sim, S.Y., Yao, Y., 2011. Interaction of solitary waves with emergent, rigid vegetation. Ocean. Eng. 38 (10), 1080–1088.

Hui, E.Q., Hu, X.E., Jiang, C.B., Zhu, Z.D., 2010. A study of drag coefficient related with vegetation based on the flume experiment. J. Hydrodyn. 22, 329–337.

Ishikawa, Y., Mizuhara, K., Ashida, S., 2000. Effect of density of trees on drag exerted on trees in river channels. J. For. Res. 5, 271–279.

Jacobsen, N., Bakker, W., Uijttewaal, W., Uittenbogaard, R., 2019. Experimental investigation of the wave-induced motion of and force distribution along a flexible stem. J. Fluid Mech. 880, 1036–1069.

Jadhav, R.S., 2012. Field Investigation of Wave and Surge Attenuation in Salt Marsh Vegetation and Wave Climate in a Shallow Estuary, vol. 3939. LSU Doctoral Dissertations.

Jeon, H.S., Hur, D.S., Park, J.R., Yoon, J.S., Kim, I.H., Lee, W.D., 2018. 3-D numerical investigation on effect of flow structure and water level on vegetation distribution in an open channel. J. Coast Res. 85, 71–75.
Kobayashi, N., Raichle, A., Asano, T., 1993. Wave attenuation by vegetation. J. Waterw. Port, Coast. Ocean Eng. 119 (1), 30–48.
Koch, E., Barbier, E., Silliman, B., Reed, D., Perillo, G., Hacker, S., Granek, E., Primavera, J., Muthiga, N., Polasky, S., Halpern, B., Kennedy, C., Kappel, C., Wolanski, E., 2009. Non-linearity in ecosystem services: temporal and spatial variability in coastal protection. Front. Ecol. Environ. 7, 29–37.
Kothyari, U.C., Hayashi, K., Hashimoto, H., 2009. Drag coefficient of unsubmerged rigid vegetation stems in open channel flows. J. Hydraul. Res. 47 (6), 691–699.
Lei, J., Nepf, H., 2019. Wave damping by flexible vegetation: connecting individual blade dynamics to the meadow scale. Coast Eng. 147, 138–148.
Loboda, M.A., Karpinski, M., Bialik, R.J., 2018. On the relationship between aquatic plant stem characteristics and drag force: is a modeling application possible? Water 10, 540.
Lou, S., Chen, M., Ma, G., Liu, S., Zhong, G., 2018. Laboratory study of the effect of vertically varying vegetation density on waves, currents and wave-current interactions. Appl. Ocean Res. 79, 74–87.
Luhar, M., Nepf, H., 2016. Wave-induced dynamics of flexible blades. J. Fluid Struct. 61, 20–41.
Maun, M.A., 1998. Adaptations of plants to burial in coastal sand dunes. Can. J. Bot. 76 (5), 713–738.
Méndez, F.J., Losada, I.J., Losada, M.A., 1999. Hydrodynamics induced by wind waves in a vegetation field. J. Geophys. Res. 104 (C8), 18383–18396.
Möller, I., Kudella, M., Rupprecht, F., Spencer, T., Paul, M., van Wesenbeeck, B.K., Wolters, G., Jensen, K., Bouma, T.J., Miranda-Lange, M., Schimmels, S., 2014. Wave attenuation over coastal salt marshes under storm surge conditions. Nat. Geosci. 7, 727–731.
Morison, J.R., O'Brien, M.P., Johnson, J.W., Schaaf, S.A., 1950. The Force Exerted by Surface Waves on Piles. Petroleum Transactions, vol. 189. American Institute of Mining Engineers, pp. 149–154.
Myrhaug, D., 2019. Random wave-driven drag forces on near-bed vegetation in shallow water based on deepwater wind conditions. Journal of Engineering for the Maritime Environment 233 (4), 1287–1290.
Naveed, M., Brown, L.K., Raffan, A.C., George, T.S., Bengough, A.G., Roose, T., Sinclair, I., Koebernick, N., Cooper, L., Hallett, P.D., 2018. Rhizosphere-scale quantification of hydraulic and mechanical properties of soil impacted by root and seed exudates. Vadose Zone J. 17, 170083.
Odériz, I., Knöchelmann, N., Silva Casarin, R., Feagin, R.A., Mendoza, E., Martínez, M., Brühl, Schürenkamp, D., 2020. Erosion and energy dissipation by reinforced dunes: an ecologically enhanced rocky infrastructure solution. Coast Eng. 158 (in press).
Paul, M., Amos, C.L., 2011. Spatial and seasonal variation in wave attenuation over Zostera noltii. J. Geophys. Res. 116, C08019.
Peruzzo, P., De Serio, F., Defina, A., Mossa, M., 2018. Wave height attenuation and flow resistance due to emergent or near-emergent vegetation. Water 10 (4), 402.
Pinsky, M.L., Guannel, G., Arkema, K.K., 2013. Quantifying wave attenuation to inform coastal habitat conservation. Ecosphere 4 (8), 95.
R Core Team, 2019. R: A Language and Environment for Statistical Computing. R Foundation for Statistical Computing, Vienna, Austria. URL. https://www.R-project.org/.
Rasband, W.S., ImageJ, U.S., 1997-2018. National Institutes of Health. Bethesda, Maryland, USA. https://imagej.nih.gov/ij/.
Roelvink, D., Reniers, A., van Dongeren, A., van Thiel de Vries, J., McCall, R., Lescinski, J., 2009. Modelling storm impacts on beaches, dunes and barrier islands. Coast Eng. 56 (11–12), 1133–1152.
Sigren, J.M., Figlus, J., Highfield, W., Feagin, R.A., Armitage, A.R., 2018. The effects of coastal dune volume and vegetation on storm-induced property damage: analysis from Hurricane Ike. J. Coast Res. 34 (1), 164–173.
Tanaka, N., Takenaka, H., Yagisawa, J., Morinaga, T., 2011. Estimation of drag coefficient of a real tree considering the vertical stand structure of trunk, branches, and leaves. Int. J. River Basin Manag. 9 (3/4), 221–230.
Temmerman, S., Meire, P., Bouma, T.J., Herman, P.M.J., Ysebaert, T., De Vriend, H.J., 2013. Ecosystem-based coastal defense in the face of global change. Nature 504 (7478), 79–83.
Thompson, A.M., Wilson, B.N., Hustrulid, T., 2003. Instrumentation to measure drag on idealized vegetal elements in overland flow. Transactions of the ASEA 46 (2), 295–302.
Tsakiri, M., Prinos, P., Koftis, T., 2016. Numerical simulation of turbulent exchange flow in aquatic canopies. J. Hydraul. Res. 54 (2), 131–144.
Vanegas, C.A., Osorio, A.F., Urrego, L.E., 2019. Wave dissipation across a Rhizophora mangrove patch on a Colombian Caribbean Island: an experimental approach. Ecol. Eng. 130, 271–281.
Vogel, S., 1984. Drag and flexibility in sessile organisms. Am. Zool. 24 (1), 37–44.
Vuik, V., Jonkman, S.N., Borsje, B.W., Suzuki, T., 2016. Nature-based flood protection: the efficiency of vegetated foreshores for reducing wave loads on coastal dikes. Coast Eng. 116, 42–56.
Warner, J., Armstrong, B., He, R., Zambon, J., 2010. Development of a Coupled Ocean-Atmosphere-Wave-Sediment transport (COASWST) modeling system. Ocean Model. 35, 230–244.
Williams, S.J., Gutierrez, B.T., 2009. Sea-level rise and coastal change: causes and implications for the future of coasts and low-lying regions. Shore Beach 77 (4), 13–21.
Wilson, C.A.M.E., Hoyt, J., Schnauder, I., 2008. Impact of foliage on the drag force of vegetation in aquatic flows. J. Hydraul. Eng. 134 (7), 885–891.
Wunder, S., Lehmann, B., Nestmann, F., 2011. Determination of the drag coefficients of emergent and just submerged willows. Int. J. River Basin Manag. 9, 231–236.
Yin, Z., Wang, Y., Yang, X., 2019. Regular wave run-up attenuation on a slope by emergent rigid vegetation. J. Coast Res. 35 (3), 711–718.
Zhang, M., Zhang, H., Zhao, K., Tang, J., Qin, H., 2017. Evolution of wave and tide over vegetation region in nearshore waters. Ocean Dynam. 67 (8), 973–988.
Zhang, H., Zhang, M., Shen, Y., Xu, T., 2020. Numerical investigation on coastal inundation of storm surges in estuarine wetland waters. J. Coast Res. 95, 1383–1388.
Zhu, L., Huguenard, K., Zou, Q.-P., Fredriksson, D.W., Xie, D., 2020. Aquaculture farms as nature-based coastal protection: random wave attenuation by suspended and submerged canopies. Coast Eng. 160, 103737.